# Thermo-economic analysis, optimisation and systematic integration of supercritical carbon dioxide cycle with sensible heat thermal energy storage for CSP application

Dhinesh Thanganadar [a], Francesco Fornarelli [b], Sergio Camporeale [c], Faisal Asfand [d], Jonathon Gillard [a], Kumar Patchigolla [a, *]

[a] School of Water, Energy and Environment (SWEE), Cranfield University, Cranfield, MK43 0AL, UK
[b] Dept. of Sciences of Agriculture, Food, Natural Resources and Engineering, University of Foggiai, Italy
[c] Dipartimento di Meccanica, Matematica e Management (DMMM), Politecnico di Bari, Bari, Italy
[d] The School of Computing and Engineering, University of Huddersfield, Huddersfield, HD1 3DH, UK

## ARTICLE INFO

## ABSTRACT

Integration of thermal energy storage with concentrated solar power (CSP) plant aids in smoothing of the variable energy generation from renewable sources. Supercritical carbon dioxide (sCO2) cycles can reduce the levelised cost of electricity of a CSP plant through its higher efficiency and compact footprint compared to steam-Rankine cycles. This study systematically integrates nine sCO2 cycles including two novel configurations for CSP applications with a two-tank sensible heat storage system using a multi-objective optimisation. The performance of the sCO2 cycles is benchmarked against the thermal performance requirement of an ideal power cycle to reduce the plant overnight capital cost. The impacts of the compressor inlet temperature (CIT) and maximum turbine inlet temperature (TIT) on the cycle selection criteria are discussed. The influence of the cost function uncertainty on the selection of the optimal cycle is analysed using Monte-Carlo simulation. One of the novel cycle configurations (C8) proposed can reduce the overnight capital cost by 10.8% in comparison to a recompression Brayton cycle (C3) for a CIT of 55 °C and TIT of 700 °C. This work describes design guidelines facilitating the development/selection of an optimal cycle for a CSP application integrated with two-tank thermal storage.

## 1. Introduction

Renewable energy technologies including concentrated solar power (CSP) plants have a significant role to play in keeping the global average temperature increase below 2 °C according to Paris agreement. CSP plants are capital intensive, but with essentially no fuel cost, consequently, the levelised cost of electricity (LCOE) principally depends on the capital cost and the regional solar resource [1]. The US Department of Energy (DOE) SunShot program has a goal to reduce the LCOE of CSP plants below 6¢/kWh [2], requiring a power block target performance of >50% efficiency with dry cooling at 55 °C ambient temperature at a unit cost of <950 $/kWe [3]. Closed loop supercritical carbon dioxide (sCO2) Brayton cycles have been considered as a power conversion cycle for all the three technologies owing to their higher efficiency compared to steam Rankine cycles, when the turbine inlet temperature (TIT) is > 550 °C, and compact plant footprint [2,4].

sCO2 cycles are not only investigated for CSP applications but also nuclear [4], coal-fired plant [5,6], combined cycle power plant [7], waste heat recovery [8], and geothermal [9]. Numerous sCO2 cycle configurations have been proposed to meet the requirements for different applications with Crespi et al. [10] reviewing forty-two of them. Turchi et al. [11] analysed advanced sCO2 cycle configurations in order to realise the SunShot power cycle targets. Crespi et al. [12] compared twelve sCO2 cycles on the basis of efficiency and specific work diagrams, and outlined the potential areas for cycle development similar to Angelino [13]. For a given power output, maximising the efficiency aids in reducing the energy input, thereby reducing the power cycle component size, due to reduced mass flow rate, and thus capital cost [14]. Crespi et al. [15] also investigated the Overnight Capital Cost (OCC), of twelve sCO2 cycles integrated with CSP and two-tank TES systems, concluding that

**Nomenclature**

| | |
|---|---|
| CIT | Compressor Inlet Temperature |
| CSP | Concentrated Solar Power |
| C1 | Simple Recuperative Brayton Cycle (Cycle #1) |
| C2 | Simple Recuperative Brayton Cycle with Intercooler (Cycle #2) |
| C3 | Recompression Brayton Cycle (Cycle #3) |
| C4 | Recompression Brayton Cycle with Intercooler (Cycle #4) |
| C5 | Partial Cooling Brayton Cycle (Cycle #5) |
| C6 | Partial Cooling Brayton Cycle with Intercooler (Cycle #6) |
| C7 | Recompression and Cascade Brayton Cycle (Cycle #7) |
| C8 | Recompression and Cascade Brayton Cycle with Intercooling (Cycle #8) |
| C9 | Transcritical $CO_2$ Rankine Cycle (Cycle #9) |
| HT | High Temperature |
| HTR | High Temperature Recuperator |
| IC | Intercooler |
| LCOE | Levelised Cost of Electricity |
| LMTD | Log Mean Temperature Difference |
| LT | Low Temperature |
| LTR | Low Temperature Recuperator |
| MC | Main Compressor |
| MS | Molten Salt |
| MSIT | Molten Salt Inlet Temperature |
| MSOT | Molten Salt Outlet Temperature |
| NSGA | Non-dominated Sorting Genetic Algorithm |
| OCC | Overnight Capital Cost |
| PC | Precooler |
| PCC | Partial Cooling Cycle |
| PHEX | Primary Heat Exchanger |
| PR | Pressure ratio |
| PreC | Pre-compressor |
| RC | Recompressor |
| RCBC | Recompression Brayton Cycle |
| $sCO_2$ | supercritical Carbon Dioxide |
| SM | Solar Multiple |
| SRBC | Simple Recuperative Brayton Cycle |
| TET | Turbine Exhaust Temperature |
| TIT | Turbine Inlet Temperature |
| $\Delta T$ | Temperature difference across the primary heat exchanger (molten salt side), equates to the temperature difference between hot and cold storage tanks |

transcritical $CO_2$ ($tCO_2$), Allam cycle and partial cooling cycles achieved lower OCC than the highly efficient recompression cycle. Crespi et al. [16] compared the effect of cycle efficiency and temperature across solar receiver on the cost for the partial cooling cycle and $tCO_2$ cycle, concluding that $tCO_2$ achieved lower capital cost. Thanganadar et al. [14] compared the techno-economic performance of recompression, partial cooling and partial heating cycles integrated with two-tank TES and central tower CSP plant for ten different boundary conditions, concluding that partial cooling cycle remains economical for all the boundary conditions investigated. Thanganadar et al. [17] compared the design, off-design and annual performance of simple recuperative, recompression and the partial cooling cycle, concluding that the partial cooling cycle can achieve lower LCOE when operating the plant in maximum power mode. Thanganadar et al. [18] analysed the off-design performance of the recompression cycle, concluding that the capacity of the thermal energy storage system can be reduced by 25% when the compressor inlet temperature (CIT) is increased by 13 °C. Sandia National Laboratories [19] have tested a pilot $sCO_2$ facility of 520 kW$_{th}$, and other research facilities are reviewed by Lecompte et al. [20]. NREL is building a 10 MW$_e$ plant which is designed to operate at a TIT of 716 °C [21].

The power cycle accounts for 10−30% of the overall plant capital cost whilst the solar field represents about 50−60% in a central power tower CSP plant [22]. The storage material cost of the two-tank sensible heat storage system is about half of the total cost of TES system [23]. For a given power output, the solar field cost decreases with increases in power block efficiency since the thermal rating of the solar receiver and the number of heliostats decreases [24]. The cost of a sensible heat two-tank storage system increases with the reduction in the temperature difference between the hot and cold tank storage temperature (denoted as $\Delta T$ hereafter) and power block efficiency as they dictate the amount of storage inventory required for a given number of storage hours [14,15]. It is clear that maximising the power cycle efficiency reduces the cost of both solar field and TES, although maximising the $\Delta T$ primarily reduces the cost of TES, when neglecting the second order effect of reduction in receiver loss owing to the lower receiver mean temperature. Conversely, maximising the $\Delta T$ penalizes the real power cycle efficiency as only a small fraction of the heat is available at the maximum temperature, reducing the Carnot mean heat addition temperature. This implies that maximum $\Delta T$ cannot guarantee cost reduction as it negatively impacts the power cycle efficiency, indicating that there should be an optimum $\Delta T$, at which the effect on efficiency is smaller, but the total cost of TES and solar field is minimised, purely dictated by the cost share of TES and solar field. Therefore, an ideal power cycle for minimising the capital cost (CC) of the CSP plant will have maximum efficiency at a $\Delta T$ close to the optimal heat addition $\Delta T$ dictated by the cost functions of the solar field and TES. In addition, the specific power of the power cycle must be larger in order to reduce the capital cost of the power block, which contributes about 10−30% of the total CSP plant CC. The SunShot program target for the power block only enforces the power block efficiency and power block unit cost and does not explicitly target the temperature difference between the two storage tanks despite its significant impact on the cost of the TES system [3]. The first part of this paper provides an methodology to estimate the optimal heat addition $\Delta T$ for a given cost functions.

Dunham et al. [25] investigated six power cycle configurations/fluids, concluding that the $sCO_2$ recompression cycle offers higher efficiency above 600 °C. Johnson et al. [26] have developed and patented a novel $sCO_2$ cycle configuration derived from the cascade cycle configurations that have a higher temperature difference across the primary heat exchanger (denoted as $\Delta T$ henceforth) in order to realise a lower LCOE. Thanganadar et al. [7] integrated five cascade cycle configurations with a bottoming cycle, and the study has shown that cascade cycles can be integrated with a sensible heat source having a larger heat addition $\Delta T$. Increasing the power cycle heat addition $\Delta T$ for a given TIT can be achieved by increasing the cycle pressure ratio, or advanced $sCO_2$ cycles derived from cascade [27] or condensed cycle ($tCO_2$) configurations [28]. Since the critical temperature and pressure of $CO_2$ is 30.98 °C and 7.38 MPa, it is not feasible to directly condense the cycle at 55 °C ambient condition (i.e. at the SunShot target). SCARABEUS [29] is an active European research project exploring $sCO_2$ blends that increase the critical temperature to enable the condensing cycle.

However, the development of novel sCO$_2$ cycles derived from cascade cycles are seldom studied for CSP applications, except for the patented configuration by Johnson et al. [26]. Crespi et al. [30] showed that higher system pressure contributes more to increasing the thermal and economic performances than higher peak temperature cycle, concluding that a bulkier high pressure resistant system is more favourable. However, the development of novel sCO$_2$ cycle configurations that maximise the cycle pressure ratio for CSP applications and their economic impact on the plant LCOE is seldom studied. The $\Delta T$ of the recompression cycle is lower (220 °C), whereas it is as high as 285 °C for the simple recuperative cycle and partial cooling cycle when the turbine inlet temperature and pressure are 750 °C and 300 bar respectively [15]. Clementoni et al. [31,32] investigated the effect of compressor inlet temperature (CIT) on the performance of sCO$_2$ cycles, which is highly sensitive to ambient temperatures. Asfand et al. [33] integrated an absorption chiller with the simple recuperative Brayton cycle (SRBC) to cool the cooling water so that the efficiency penalty at a higher temperature can be reduced. The compressor inlet pressure has to be close to the (pseudo) critical pressure for different compressor inlet temperatures so that the compressive power is minimised, in turn maximising the efficiency [34]. Since the pseudo critical pressure increases with temperature, the cycle pressure ratio reduces for a given cycle maximum pressure economical limit (around 250−300 bar) when the compressor inlet temperature increases [15]. Consequently, the differential temperature across the primary heat exchanger reduces at higher ambient temperatures. Therefore, at a higher ambient temperature, the capital cost will increase not only due to the reduction in efficiency but also the TES cost owing to the reduction in $\Delta T$. However, to the best of the author's knowledge, the effect of the ambient temperature and TIT on the plant capital cost and the requirements on power cycle design to reduce the cost has not been investigated.

This paper aids in selecting the best power cycle configuration and design point based on the optimal heat addition $\Delta T$ that minimises the cost of both solar field and TES. This paper also investigates the thermodynamic performance of nine sCO$_2$ cycles, of which two novel cycle configurations derived by combining the features of recompression and cascade cycles, with the objective of maximising the efficiency and heat addition $\Delta T$, are also investigated. The effect of ambient temperature on the selection of cycle configuration for two different turbine inlet temperatures (600 °C and 700 °C) are investigated using multi-objective optimisation techniques for the first time. The cycle configurations are systematically integrated with a central power tower and two-tank sensible heat storage system with the goal of minimising the overall capital cost and they are compared against the optimal heat addition $\Delta T$ derived from an ideal power cycle for a 50 MW$_e$ plant. Finally, a Monte-Carlo simulation is performed in order to account the uncertainty of all the cost functions on the cycle and design point selection.

## 2. sCO$_2$ cycle configurations

All nine cycle configurations studied are shown in Fig. 1 and the cycle naming convention is shown in Table 1. The simple recuperative cycle (C1) is a closed-loop recuperated Brayton cycle and for C2, a two-stage intercooled compressor is considered. The recompression cycle (C3) recuperates more heat than C1 by splitting the recuperator into two and controlling the cold stream mass flow through the low-temperature recuperator (LTR), which eventually eliminates the pinch limitation that occurs in C1 and C2. C4 adds an intercooler to the recompression cycle (C3). The partial cooling cycle (C5) partially cools the hot stream return from the LTR to a superheated state, then pre-compresses the CO$_2$ above the critical

point. Part of the flow bypasses the LTR via the recompressor whist the remaining flow goes through the cooler and main compressor. The high-temperature side processes of C5 are similar to C3 and C4. Cycle C6 replaces the pre-compressor and the main compressor with two-stage intercooled compressors. Because of the added intercooler in the pre-compressor, the minimum pressure of the cycle is allowed to drop to 30 bar for the optimisation. C7 is derived by combining the recompression cycle and cascade cycle [7]. In this configuration, the PHEX is split into two with the low temperature PHEX adding heat parallel to the HTR while mass flow to the high temperature PHEX is controlled by branching off some flow through a low temperature turbine. C8 adds a two-stage compression to the main compressor loop with an intercooler. C9 is the transcritical CO$_2$ cycle which condenses at the heat rejection unit. Fig. 2 shows the cycle integration scheme with the TES and CSP plant using C3 as an example.

The PHEX is heated via hot molten salt from the solar field. The precooler is a direct air-cooled type with a pinch of 15 °C whilst the recuperator and the primary heat exchangers are compact Printed Circuit Heat Exchangers (PCHE). All the nine process configurations are simulated and optimised using a flexible in-house sequential based solver [17,18] (details together with additional validation can be found in the supplementary materials). The thermal physical properties of sCO$_2$ are calculated using the REFPROP V9.1 library [35]. The sCO$_2$ mass flow rate is adjusted to achieve the desired net power output from the plant (i.e. 50 MW$_e$). The molten salt mass flow rate is adjusted to match the desired pinch value in the PHEX. The cooling air mass flow is calculated using a temperature rise of 11 °C across the precooler coldstream [36]. Eutectic molten chloride salt mixture of 32% MgCl$_2$- 68% KCl (mole %) is considered as the heat transfer fluid and the sensible heat storage medium.

A Non-dominated Sorting Genetic Algorithm (NSGA-II) [37] is used which maximises the net efficiency and heat addition $\Delta T$ by optimising the power cycle process variables including pressure(s) and split fractions. Details of the process simulation algorithm (Section A), thermodynamic modelling assumptions (Section A.1), integration of multi-objective optimisation code (Section B) and the optimisation search space shall be found in the supplementary materials. The cost functions of the power block components (Section C) are listed in the supplementary material [38−40], where the economic calculation of the solar field and TES is also detailed [15,41−43].

## 3. Results and discussion

### 3.1. Optimal heat addition $\Delta T$ for an ideal power cycle

The power cycle efficiency can be assumed as a factor of the Carnot efficiency $(1 - \frac{T_{sink}}{T_{source}})$, where the factor is denoted as the Carnot factor [15]. Since the heat addition process is isothermal in an ideal Carnot process, the Carnot efficiency is independent of the heat addition $\Delta T$, however, achieving the same power cycle efficiency in reality at a higher heat addition $\Delta T$ for a given maximum temperature is highly unlikely as only a small proportion of the heat is supplied at the maximum temperature. Therefore, Lorenz efficiency [44] $(1 - \frac{T_{sink}}{T_{source,avg}})$, also referred to as equivalent Carnot efficiency, calculated based on mean-effective temperature [45] is adopted in this work where the heat is added over a temperature range (heat addition $\Delta T$). Power block efficiency is calculated using Eq. (1) as some fraction of the Lorenz efficiency, referred to as the Lorenz factor $(f_{LZ})$ in this work, where the average temperature $(T_{h,avg})$ is the log-mean temperature, calculated using Eq. (2) [45].
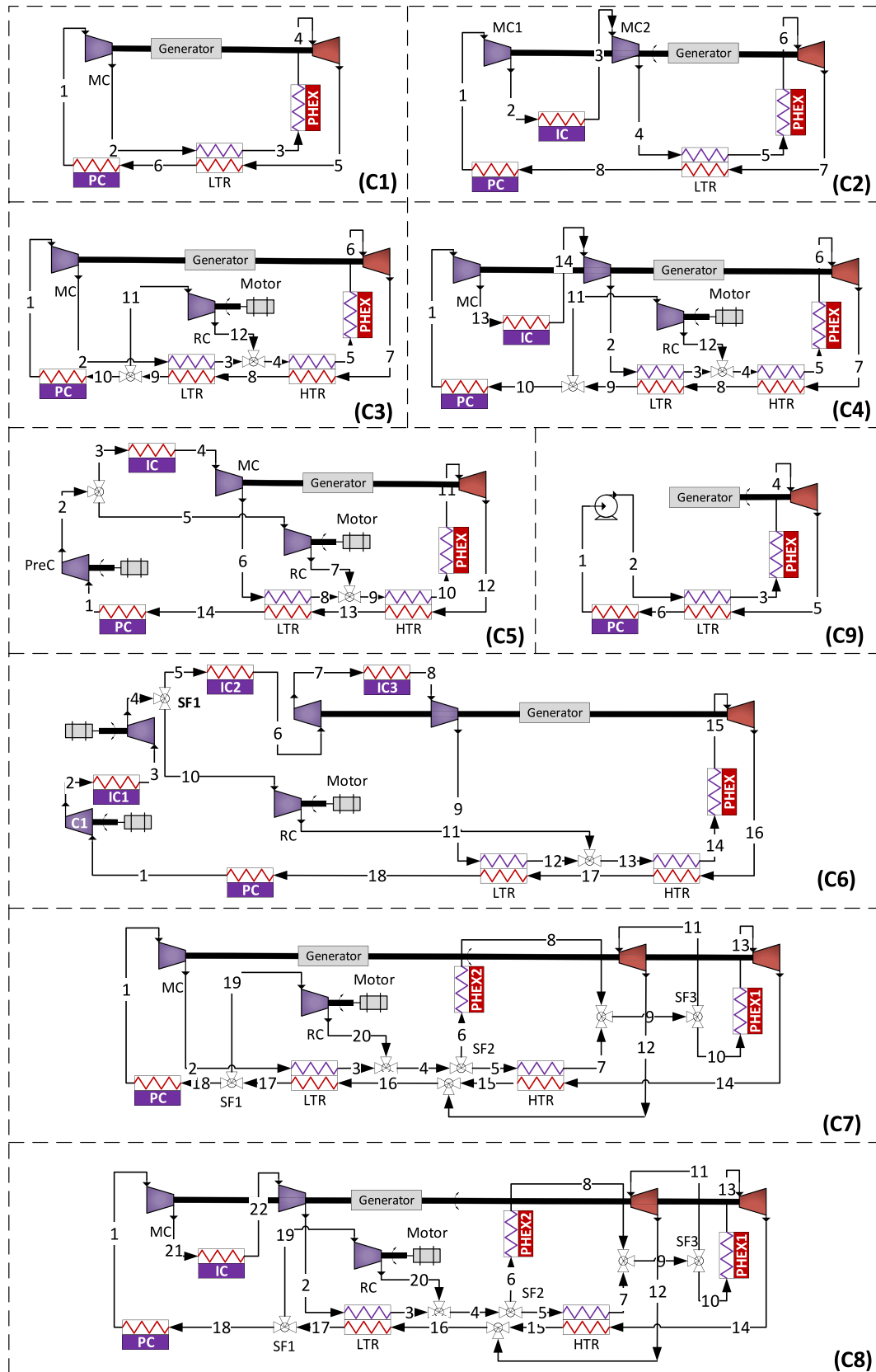
Fig. 1. sCO$_2$ cycle configurations.

**Table 1**
Cycle configuration considered in this study.

| Cycle Code | Name | Acronym |
|---|---|---|
| **C1** | Simple recuperative Brayton cycle | SRBC |
| **C2** | Simple recuperative Brayton cycle with intercooling | SRBC + IC |
| **C3** | Recompression cycle | RCBC |
| **C4** | Recompression cycle with intercooling | RCBC + IC |
| **C5** | Partial cooling cycle | PCC |
| **C6** | Partial cooling cycle with intercooling | PCC + IC |
| **C7** | Recompression-Cascade cycle | RCBC + Cascade |
| **C8** | Recompression-Cascade cycle with intercooling | RCBC + Cascade + IC |
| **C9** | Transcritical $CO_2$ cycle | $tCO_2$ |
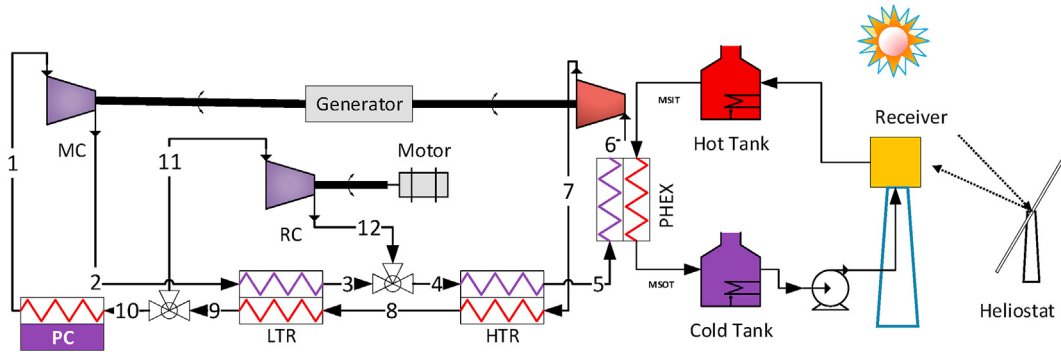


**Fig. 2.** Simplified Cycle Integration Scheme with CSP and TES systems (C3 is shown as an example).

$$\eta_{PB,i} = f_{LZ} \times \left(1 - \frac{T_c}{T_{h,avg}}\right) \tag{1}$$

$$T_{h,avg} = \frac{T_{h,in} - T_{h,out}}{\ln(T_{h,in}) - \ln(T_{h,out})} \tag{2}$$

The outlet temperature of the PHEX ($T_{h,out}$) is dictated by the $T_{h,in}$ and heat addition $\Delta T$ ($T_{h,in} - T_{h,out}$). The unit cost of the solar field and TES system assuming Carnot and Lorenz factors of 0.7 are plotted in Fig. 3. It is clear that a fixed Carnot factor always reduces the unit cost with an increase in heat addition $\Delta T$ owing to the reduction in the TES cost as the cycle efficiency is independent of heat addition $\Delta T$. On the other hand, assuming a fixed Lorenz factor

also affects the cycle efficiency, consequently there is an optimal heat addition $\Delta T$ after which the reduction in the cost of TES is outweighed by the increase in cost due to the power cycle efficiency (Fig. 4).

The optimum heat addition $\Delta T$, at which the unit cost of the solar field and TES reduces, can vary depending on many factors including the cost functions, source temperature, sink temperature, Lorenz factor (efficiency), power plant size, solar multiple and storage hours. Fig. 5 shows how the unit cost varies with heat addition $\Delta T$ for two different source and sink temperatures. Since the unit cost of the solar field and TES curve is plateaued over a large temperature difference near the minimum cost point, the range of heat addition $\Delta T$ where the cost is lower than 101% of the minimum value is shown in Table 2 (denoted as upper and lower
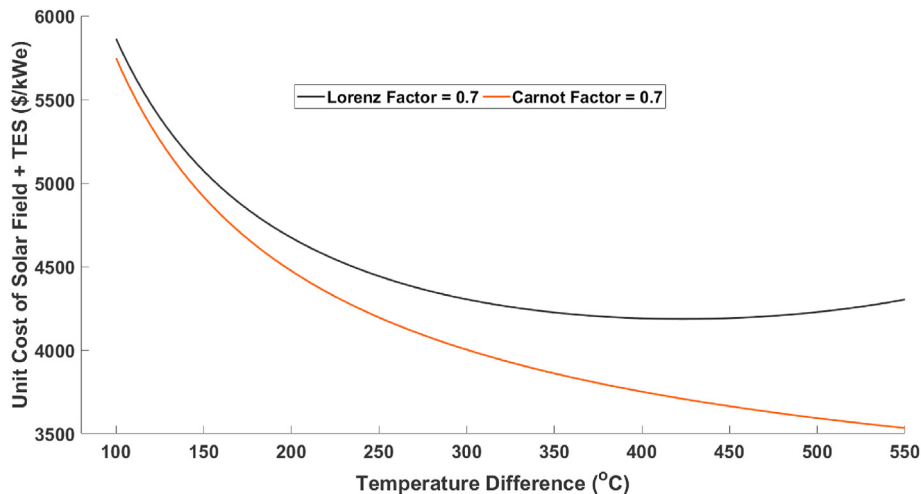


**Fig. 3.** Unit cost of solar field and TES with Carnot factor of 0.7 and Lorenz factor of 0.7, SM = 2.4, TES = 10hrs, plant size = 50 MW$_e$, TIT = 700 °C, CIT = 32 °C.
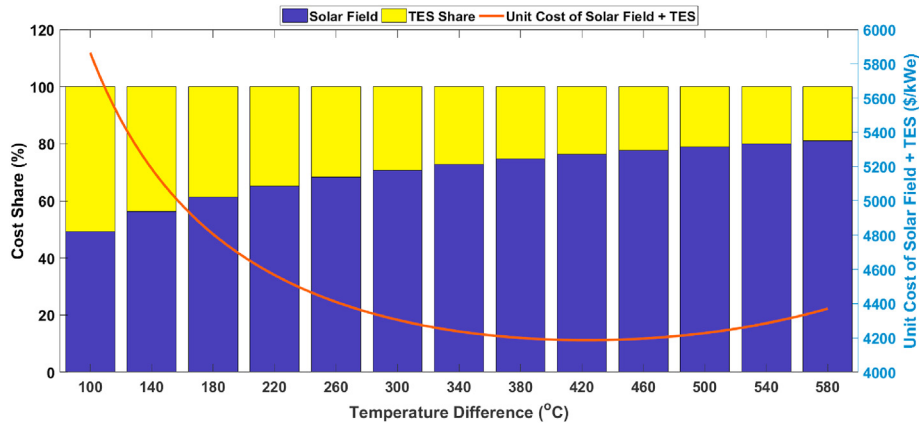
**Fig. 4.** Cost Share and total unit cost of solar field + TES, Lorenz factor = 0.7, SM = 2.4, TES = 10hrs, plant size = 50 MW$_e$, TIT = 700 °C, CIT = 32 °C.
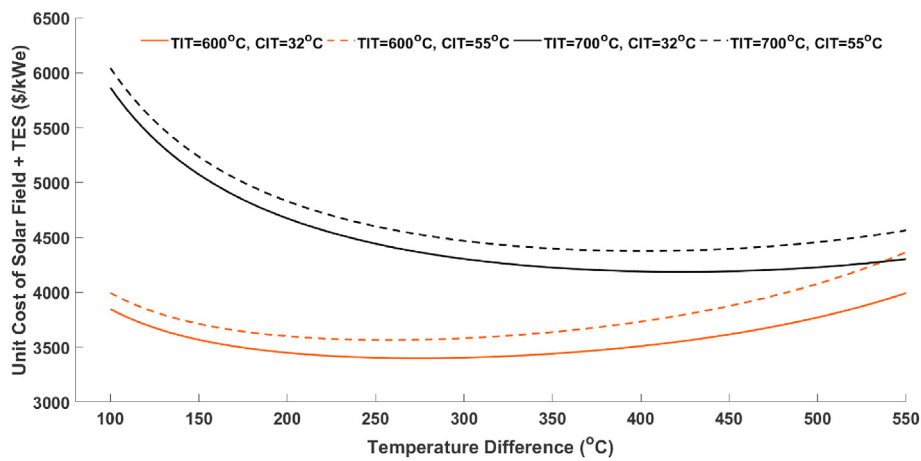


**Fig. 5.** Total unit cost of solar field + TES for different CIT and TIT, Lorenz factor = 0.7.

bound of optimal heat addition ΔT henceforth). The ideal power cycle has to achieve the maximum efficiency proximate to the optimal heat addition ΔT in order to realise the maximum cost reduction potential for given cost functions. Increasing the Lorenz factor, which also increases the efficiency linearly for a given heat addition ΔT (Eq. (1)), always reduces the solar field and TES system integration cost. For a power block at either the upper or lower bound optimal heat addition ΔT to reduce the minimum integra-tion cost by 1%, necessitates either >5% power block cost reduction (assuming that the power cycle is 20% of total plant cost) to realise cost reduction at the plant level when the Lorenz factor is

**Table 2**
Optimal heat addition ΔT for different TIT and CIT.

| Lorenz Factor | TIT (°C) | CIT (°C) | Optimal heat addition ΔT (min bound-max bound) (°C)[a] |
|---|---|---|---|
| 0.7 | 600 | 32 | 274 (212−343) |
| 0.7 | 600 | 55 | 257 (200−322) |
| 0.7 | 700 | 32 | 423 (348−500) |
| 0.7 | 700 | 55 | 401 (330−474) |
| 0.85 | 600 | 32 | 286 (219−359) |
| 0.85 | 600 | 55 | 270 (208−338) |
| 0.9 | 700 | 32 | 436 (356−517) |
| 0.9 | 700 | 55 | 416 (341−492) |

[a] The values within the parenthesis represent the minimum and the maximum limits where the unit cost of solar field + TES is lower than 101% of the lowest value.

unaffected, or requires the Lorenz factor/efficiency to increase by >1.2% to realise cost reduction in the plant level when the power block cost is unaffected. It is clear from Table 2 that the heat addition ΔT has to be more than 274 °C for a TIT of 600 °C and about 423 °C for a TIT of 700 °C for a Lorenz factor of 0.7 which increases about 10 °C when the Lorenz factor increases to 0.85. It is also clear that the variation of the optimal heat addition ΔT is predominant for changes in maximum source temperature rather than changes in CIT (i.e. ambient temperature). This is because changes in TIT not only affects the Lorenz efficiency but also increases the storage system cost more than the increase in solar field cost (i.e. receiver cost) owing to the requirement of high-temperature materials for the hot/cold tanks. Consequently, the optimal heat addition ΔT increases further to reduce the TES system cost. The effect of Lorenz factor, plant size, cost function and TES size on the optimal heat addition ΔT is shown via a sensitivity study in the supplementary material (Section F). The optimal ΔT is less sensitive to the Lorenz factor (refer to supplementary material for more details).

### 3.2. Performance of sCO$_2$ cycles

#### 3.2.1. Comparison of cycles for a CIT of 32 °C and TIT of 600 °C

Fig. 6 shows the optimal Pareto front of the nine CO$_2$ cycles, where net efficiency and temperature difference across the PHEX (heat addition ΔT) are maximised. Although the CIT of tCO$_2$ cycle (C9) is 15 °C to ensure condensation in the precooler, they are

compared with other supercritical cycles at a CIT of 32 °C. It is worth highlighting that the cycle with maximum efficiency cannot yield a lower OCC when the heat addition ΔT deviates from the optimal heat addition ΔT obtained from the ideal cycle analysis (Table 2) unless the increased integration cost of TES and CSP from its minimum value (referred as integration penalty henceforth) is compensated by the increased cycle efficiency (Lorenz factor) or reduction in the power block specific cost. This optimal heat addition ΔT can be obtained for a given set of cost functions of the solar field and TES (relative cost weightage of solar field and TES dictates the optimal heat addition ΔT), and the effect of changes in the Lorenz factor is negligible (~10 °C). In order to achieve the lowest cost from the solar field and TES, the heat addition ΔT has to be around 280 °C for a CIT of 32 °C and TIT of 600 °C (Table 2). The optimal heat addition ΔT range listed in Table 2 is also plotted together with the Pareto front in Fig. 6 to aid in selecting the optimal cycle configuration and design points in the context of reducing the cycle integration cost penalty.

The heat addition ΔT of RCBC configurations (C3) when maximising the efficiency is roughly 70 °C lower than optimal heat addition ΔT of the ideal cycle, however, it is only about 10 °C lower, when a 1% integration penalty is allowed (Table 2). This indicates that this cycle design can only be economically attractive if the unit cost of the power cycle is low enough (about 5% power block cost) or cycle efficiency increases by 1.2% (compared to the efficiency considered in Table 2) to compensate for the increased cost from integration of TES and solar field. The heat addition ΔT approaches the optimal heat addition ΔT for C3 with a trade-off in the efficiency and this cycle efficiency penalty may be economically justified if the integration penalty is minimised by increasing the cycle heat addition ΔT. The economical optimal design point selection in the Pareto front is dictated by variation of the power cycle cost and cycle efficiency across the Pareto front. For tCO$_2$ cycle (C9), the heat addition ΔT is higher than the optimal heat addition ΔT by about 70 °C, which also penalizes the integration cost. All the nine cycle configurations studied fall within the 1% integration penalty range considered, therefore the trade-off between the power block cost and the cycle efficiency primarily controls the selection of cycle configuration and optimal design point.

The heat addition ΔT is always higher when adding an intercooler, as expected. RCBC with intercooler configuration (C4) achieved the highest efficiency of 49.4% at a heat addition ΔT of 212.2 °C, whilst the RCBC (C3) achieved an efficiency of 49.2% at 202.6 °C. C7 and C8 are also able to achieve similar maximum efficiencies, i.e. 48.8% and 49.3% respectively, by reducing to the RCBC configuration (i.e. closing the split fraction to PHEX2 and low

temperature turbine). However, the heat addition ΔT of C7 and C8 are higher than RCBC at the minimum efficiency points as they have a higher degree of freedom. These cycles also achieved higher heat addition ΔT compared to the partial cooling and tCO$_2$ cycles for a heat addition ΔT corresponding to the tCO$_2$ cycle.

Fig. 7 shows the Lorenz factor plotted across the Pareto front shown in Fig. 6, which should be interpreted together with Fig. 6. For example, the maximum efficiency point of a cycle in Fig. 6 corresponds to the minimum heat addition ΔT point in Fig. 7. The Lorenz factor decreases abruptly after a certain heat addition ΔT for C4, C5, C6, C7 and C8. Maintaining an approximately flat Lorenz factor with an increase in heat addition ΔT indicates that the reduction in cycle efficiency roughly compensates for the reduction of Lorenz efficiency (Eq. (1)), thus the Lorenz factor is plateaued. After a certain threshold, the reduction in cycle efficiency is steeper than the changes in heat addition ΔT, which reduces the Lorenz factor steeply, and it is very unlikely to justify the increase in heat addition ΔT in this regime as the efficiency penalty is dominant. The maximum Lorenz factor of RCBC (C3, C4), and PCC (C5, C6) were higher than tCO$_2$ (C9) cycle at a lower heat addition ΔT. C6 Lorenz factor is lower than tCO$_2$ at a heat addition ΔT corresponding to the tCO$_2$ cycle whilst it is slightly higher for C7 and C8 (Fig. 7).

Fig. 8 shows the OCC plotted across the Pareto front shown in Fig. 6. Recompression cycles (C3, C4) and partial cooling cycles (C5, C6) achieved a lower cost proximate to the maximum efficiency point (minimum heat addition ΔT point in Fig. 8). On the other hand, simple recuperative cycles (C1, C2) reached minimum OCC proximate to the maximum heat addition ΔT point in the Pareto front despite having lower efficiencies, where the cycle minimum pressure reaches the lower bound. This is because the Lorenz factor is not affected at higher heat addition ΔT points (Fig. 7) for SRBC whilst RCBC and PCC are significantly penalised with increases in heat addition ΔT. For C7 and C8, the minimum OCC occurs neither at the maximum efficiency point nor at the maximum heat addition ΔT point, but it lies in-between maximum efficiency and maximum heat addition ΔT. By comparing Figs. 7 and 8, it can be interpreted that the increase in heat addition ΔT to reduce the OCC is favourable as long as it doesn't notably affect the Lorenz factor significantly (neglecting the variation of power block cost), although the absolute efficiency changes (Fig. 6). The OCC of tCO$_2$ cycle is the lowest in comparison to all the other cycles i.e. 4.5% lower than the minimum OCC of RCBC, however, it should be noted that the additional cooling system cost in tCO$_2$ cycle required to achieve 15 °C at the precooler outlet is not considered here (out of the scope). The minimum OCC of SRBC is 1.1% higher than RCBC whilst for C8 it reduces by 0.6% compared to RCBC (C3). It is worth
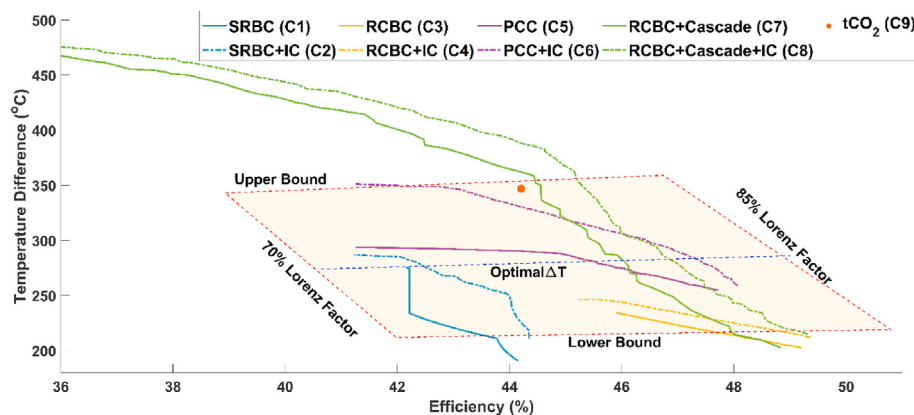
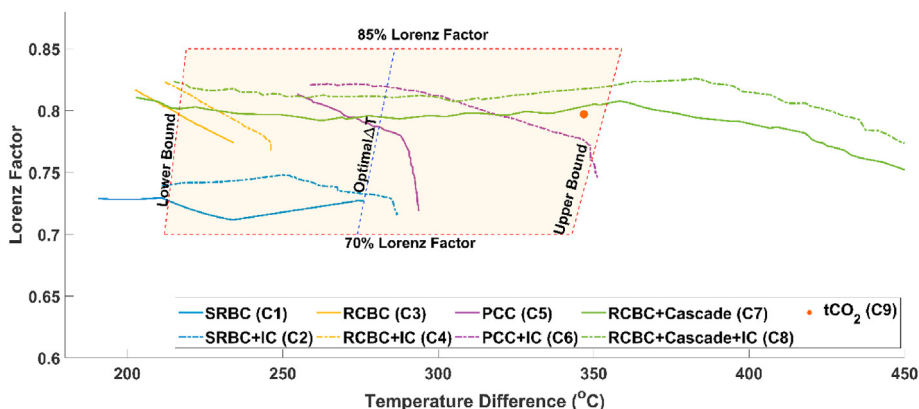**Fig. 6.** Pareto fronts obtained from NSGA-II for CIT = 32 °C and TIT = 600 °C.

**Fig. 7.** Lorenz factor across the Pareto front (shown in Fig. 6) for CIT = 32 °C and TIT = 600 °C.
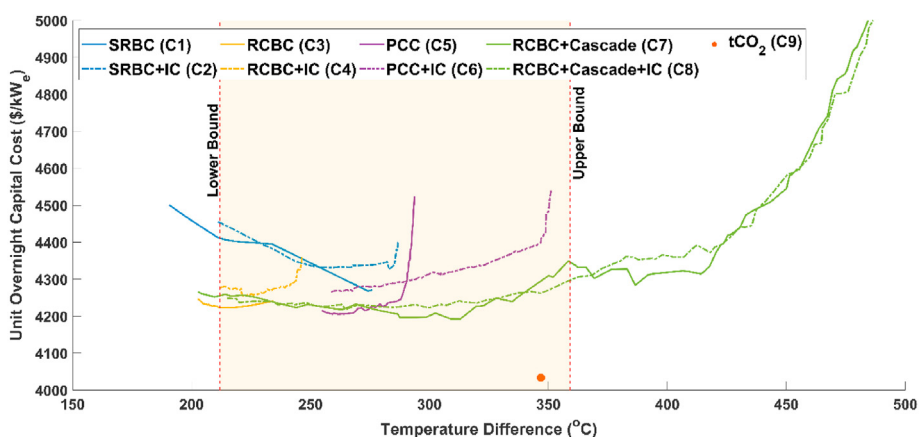


**Fig. 8.** Overnight Capital Cost across the Pareto front (shown in Fig. 6) for CIT = 32 °C and TIT = 600 °C.

highlighting that comparing the cycle configurations at their maximum efficiency point can be misleading, as it will exclude the other potential design which have better efficiency at a heat addition ΔT closed to the optimal heat addition ΔT that minimises the integration penalty. Therefore, the cycle selection process has to also consider the heat addition ΔT and Lorenz factor to screen the cycle configurations or design points obtained from thermodynamic analysis.

The OCC and the power block cost break down at the minimum OCC point for each cycle are plotted in Fig. 9 and their thermal and economic performances at the minimum OCC point are tabulated in the supplementary material (Section E.1). It should be noted that the PHEX cost dominates the power block cost in all the nine cycles studied. The cost of the PHEX of C7 and C8 are lower than other cycles mainly because the heat addition (PHEX) is split into two heat exchangers and the optimisation identified roughly equal heat duty, which lowers the temperature correction (material grade requirement) of the low temperature PHEX, whilst the entire heat addition occurs in a single heat exchanger in other cycles which consequently use high-grade material. On the other hand, the recuperator cost is higher for C7 and C8 compared to other cycles primarily due to better temperature matching between hot and cold streams, which increases the conductance owing to a reduced temperature driving force. The recuperator cost of C9 is the least because not only the heat duty is lower (higher cycle pressure ratio) but also the temperature driving force is higher. Contrarily, the cooler cost is higher in C9 due to the increased heat rejection duty (cooling to 15 °C) whilst the cooler cost of other cycles without

intercooler is dictated by the efficiency (i.e. heat rejection). TES cost share in the OCC is smaller than the contribution of power block and solar field, which indicates a further cost reduction mandates reducing the power block cost (reducing the number of components and size) and increasing the cycle efficiency without deviating from the optimal heat addition ΔT requirement.

*3.2.2. Comparison of cycles for a CIT of 32 °C and TIT of 700 °C*

The Pareto fronts for all the nine cycles are plotted in Fig. 10 for a TIT of 700 °C. Although the general trends are similar to TIT 600 °C (Fig. 6), the cycle relative positions with respect to the optimal heat addition ΔT to reduce the integration penalty is different, which can make different cycles attractive at this temperature level. For instance, the heat addition ΔT of the intercooled partial cooling cycle (C6) is the same as the tCO₂ cycle at the same efficiency level and both are close to the optimal heat addition ΔT. The heat addition ΔT of C7 and C8 are higher than tCO₂ cycle by 51 and 68 °C respectively at the same efficiency level. This implies that if the reduction in the integration penalty due to this increased heat addition ΔT is higher than the increased power block cost, resulting from the increased number of components, then C7 or C8 can be attractive.

The optimal heat addition ΔT from an ideal cycle is around 430 °C, which varies between 348 and 517 °C when considering ±1% integration penalty. Only C6, C7, C8 and C9 are able to achieve such heat addition ΔT values, even with a 1% integration penalty consideration. It should be noted that the power cycle efficiency is reduced to about 50% (C6 and C8) within the optimal heat addition
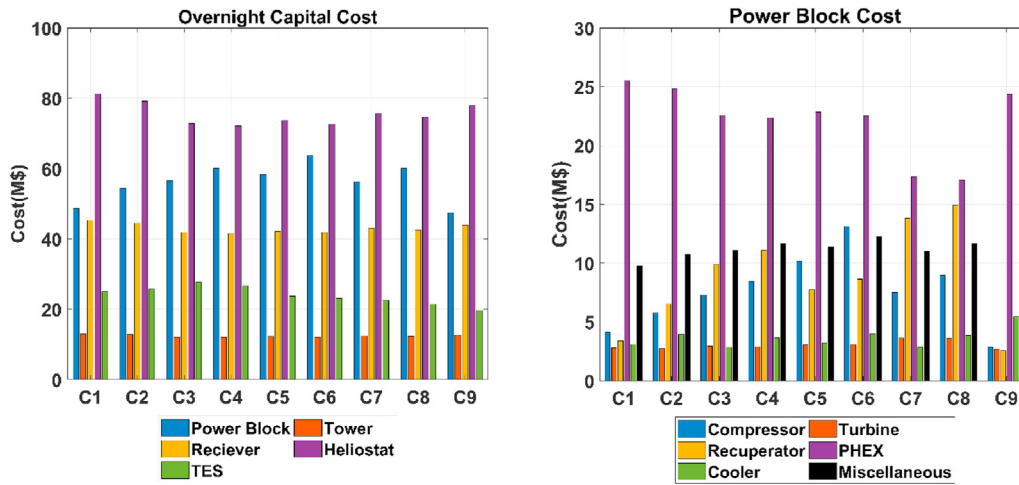
**Fig. 9.** Cost breakdown for CIT = 32 °C and TIT = 600 °C at the minimum overnight capital cost point: Left) Total capital cost Right) Power block cost breakdown.
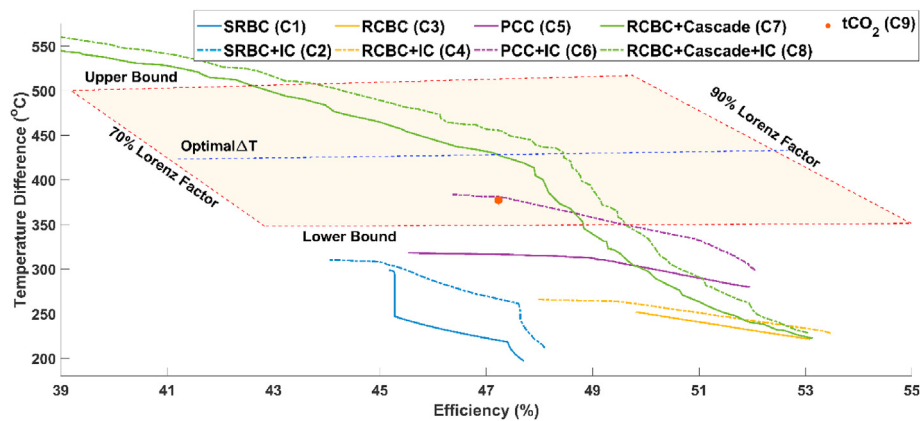


**Fig. 10.** Pareto fronts obtained from NSGA-II for CIT = 32 °C and TIT = 700 °C.

ΔT range (intersection of heat addition ΔT lower bound with the Pareto front in Fig. 10) although the maximum cycle itself can be up to 53.5% (C4). This implies that the higher efficiency cycles such as C4 need to overcome the integration penalty by the increased Lorenz factor and reduction in the power block cost in order to be economically attractive. Since the unit cost of TES and solar field (Fig. 5) monotonically increased below a heat addition ΔT of about 250 °C due to increased TES cost, any cycle configurations with lower heat addition ΔT may not achieve a reduction in OCC and therefore, the cycle configurations C3 and C4 can be omitted from further analysis. Although the heat addition ΔT of C1 and C2 can be higher than ~250 °C, this is achieved at a lower efficiency point which indicates that the power cycle cost reduction is overcome by the integration penalty, which makes these cycles uncompetitive as well. Fig. 11 shows the Lorenz factor across the Pareto front. C7, C8 and intercooled partial cooling cycle (C6) are higher than tCO₂ cycle, whereas the other cycles have a lower heat addition ΔT compared to the tCO₂ cycle.

The OCC is plotted in Fig. 12 and the cost of cycles C7 and C8 are almost the same as the cost of the tCO₂ cycle. This is equivalent to an OCC reduction of 6.3% compared to the minimum cost of RCBC (C3). It is evident that the optimal economic cycle selection also depends on the maximum operating temperature as the same C7 and C8 configurations were not economically optimal for a TIT of 600 °C. The primary driver for this is the dramatic increase in the

TES system cost in comparison with the cost of the solar field, which shifts the optimal heat addition ΔT higher. Conversely, the intercooled partial cooling cycle (C6) OCC is still 4.1% higher than that of the tCO₂ cycle. From a thermal performance perspective (Lorenz factor and heat addition ΔT), this cycle has equivalent characteristics to the tCO₂ cycle, yet the overall cost is higher due to the increase in power block cost. Although C7 and C8 layout have more components than the partial cooling cycle, their costs are equivalent to the tCO₂ cycle due to 1) increased Lorenz factor and 2) reduced power block cost due to lower PHEX cost.

The thermal and economic performances at the minimum OCC point are tabulated in the supplementary material (Section E.2). From Fig. 13, it can be observed that although the increase in the molten salt inlet temperature increases the power block efficiency, reducing the heat duty of the PHEX for a given net electric power output, the cost of the PHEX is slightly higher than the equivalent 600 °C case owing to the high temperature material. On the other hand, the cooler cost reduces in all the cycles owing to the reduced amount of heat rejection. For the same turbine shaft power the turbine cost increases by a factor of 2.73 when the TIT increases from 600 to 700 °C. Likewise, the turbine cost of all the cycles has increased significantly (100−170% compared to 600 °C cases) despite increasing the specific power of the cycle and reducing the absolute turbine shaft power, whilst the cost of the compressor(s) is lower than 600 °C cases. Overall, the power block cost has
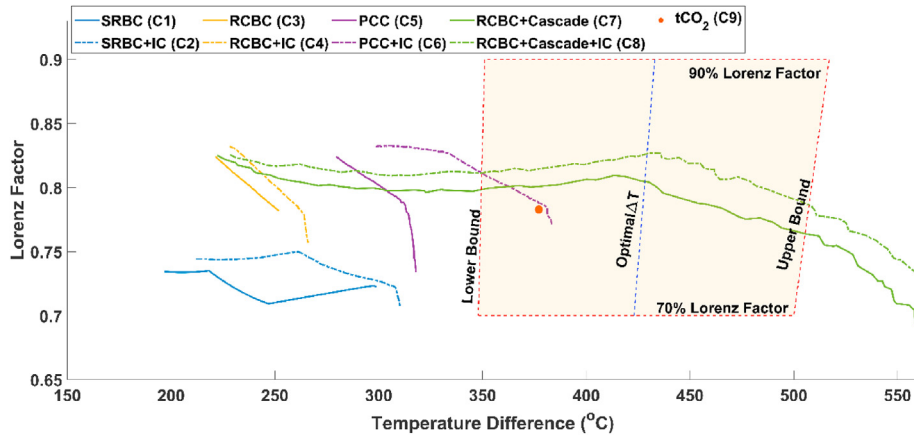
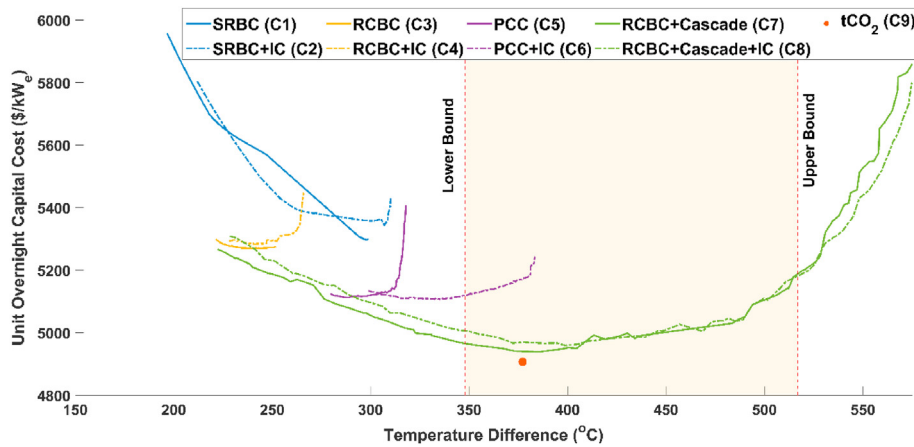**Fig. 11.** Lorenz factor across the Pareto front (shown in Fig. 10) for CIT = 32 °C and TIT = 700 °C.



**Fig. 12.** Overnight capital cost across the Pareto front (shown in Fig. 10) for CIT = 32 °C and TIT = 700 °C.
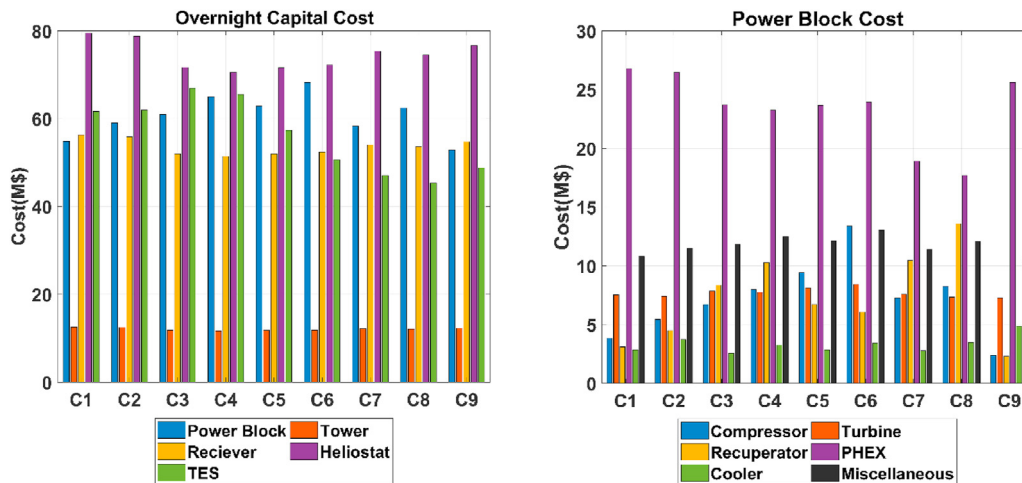


**Fig. 13.** Cost breakdown for CIT = 32 °C and TIT = 700 °C at the minimum overnight capital cost point: Left) Total capital cost Right) Power block cost breakdown.

increased by 11.5% for C9 but it is only increased by 3.9% for C8. The cost of TES increased by 109.3% and 111.6% for C8 and C9, respectively. The receiver cost increased by about 25.7% with a slight reduction in the tower cost (~2.5%). The heliostat cost of C8 and C9 has not reduced with the increase in temperature from 600 to

700 °C as the increased power cycle efficiency is balanced by the increased receiver loss at a higher temperature. However, a reduction of about 2.3% is realised for C4 owing to the highest power cycle efficiency. This leads to an increase in OCC by 17.5% and 17.7% for C7 and C8, respectively. Despite increasing the cycle

efficiency, increase in power cycle TIT does not offer any reduction, neither in the cost of power block nor in the OCC, instead it increased both for all the cycles studied, for example, $tCO_2$ cycle OCC increased by 21.7%. This suggests that 600 °C operation can be favoured purely from an economical perspective. The future developments in order to reduce the OCC should either 1) develop a novel cycle with higher efficiency proximate to the optimal heat addition $\Delta T$ without increasing the power block unit cost, or 2) reduce the cost of high temperature TES system so that the optimal heat addition $\Delta T$ requirement is reduced, in which case the integration penalty of the $sCO_2$ cycles can be lowered. It is worth highlighting that selection of cycle configuration based on efficiency favours C4, but the OCC at the maximum efficiency point is higher than the minimum OCC of C9 by 7.7% and therefore, the optimal heat addition $\Delta T$ should be considered.

### 3.2.3. Comparison of cycles for a CIT of 55 °C and TIT of 600 °C

In order to understand the effect of CIT in the cycle selection, the optimisation is repeated for a 55 °C CIT and the Pareto fronts are shown in Fig. 14. It has to be noted that the $tCO_2$ cycle is not simulated as condensing $CO_2$ at a higher temperature demands blending fluid mixtures to increase the critical temperature, which is out of the scope of this study. The maximum cycle efficiency of all the eight cycles is reduced by the increase in CIT within a range of 3−4.3% point. The maximum heat addition $\Delta T$ also reduces for all the cycles as the increase in CIT also increases the cold stream inlet temperature to the recuperator, thereby increasing the cold inlet temperature of the PHEX. On the other hand, the increase in heat addition $\Delta T$ by the addition of intercooler for a CIT = 55 °C is higher than the equivalent cases for a CIT of 32 °C. For example, the heat addition $\Delta T$ at the maximum efficiency point of SRBC with intercooler (C2) is higher than SRBC (C1) by 38.4 °C whereas it increased only by 20.4 °C for a CIT of 32 °C. The optimal heat addition $\Delta T$ of an ideal cycle is around 265 °C as depicted in Table 2 (200−338 °C considering ±1% integration penalty) and all of the cycle configurations except C1 and C3 are able to achieve this level of heat addition $\Delta T$. The heat addition $\Delta T$ of C2 is proximate to the optimal heat addition $\Delta T$ values at the maximum efficiency point, which infers that this cycle configuration can be better if the absolute lower efficiency offsets the increased solar field and TES cost. On the other hand, the heat addition $\Delta T$ of C3 is lower than the optimal heat addition $\Delta T$, yet the higher efficiency could potentially offset the integration penalty. Therefore, all the cycle configurations except C1 can be considered for detailed investigation.

The Lorenz factor across the Pareto front is shown in Fig. 15 and they are lower than the equivalent factors for a CIT of 32 °C. The

Lorenz factor of partial cooling cycle with intercooler (C6) reaches a higher value than C7 and C8 proximate to the optimal heat addition $\Delta T$, which indicates that C6 will reduce the integration penalty and this cycle can be attractive if the power block unit cost is not significantly higher.

The OCC of all the cycles are shown in Fig. 16 and it can be clearly seen that the addition of an intercooler with SRBC (C1), RCBC (C3), PCC (C5) and C7 reduce the OCC by 3.2, 3.2, 0.3 and 2% respectively, which is expected from their increased thermal performance. C6 and C8 show similar minimum OCC (OCC of C6 is 0.7% higher than C8) at around 257 and 261 °C heat addition $\Delta T$ respectively, therefore C6 is attractive over C8 owing to its lower complexity. It is worth highlighting that C6 was not economically attractive for a CIT of 32 °C, however, the OCC of C5, C4 and C2 also reached similar OCC as C6 configuration, which indicates that C2 can be economically attractive owing to its simpler configuration with a lower number of components. The reduction of efficiency with the increase in CIT from 32 to 55 °C contribute to an increase of OCC by 8.1% and 10.4% for C2 and C8 respectively.

The heat duty of the PHEX and cooler (Fig. 17) have increased from their corresponding values for a CIT of 32 °C in the range of 10.6% (C1) and 14% (C5). Despite increasing the cooler heat duty, the cost of the cooler for all the eight cycles has decreased compared with a CIT of 32 °C owing to the increased temperature driving force. The compressor shaft power increases for CIT of 55 °C, which also increased the cost of the compressor for all the cycles in the range of 10.3% (C7) to 29.6% (C1). The cost of the turbine has also increased as the increased compressor shaft power (6−12.4%) is supplied from the turbine. Overall, this increases the power block cost in a range from 8.9% (C8) to 13.8% (C3) compared to a CIT 32 °C. The TES cost also increases from a minimum of 13.2% (C8) to a maximum of 38.3% (C1) due to both drop in efficiency and heat addition $\Delta T$. The performance summary at the minimum OCC point are tabulated in the supplementary material (Section E.3).

### 3.2.4. Comparison of cycles for a CIT of 55 °C and TIT of 700 °C

The Pareto fronts that maximise both efficiency and heat addition $\Delta T$ are plotted in Fig. 18. The maximum efficiency of the cycle has increased from a minimum of 3.5% point (C1) to a maximum of 4.9% point (C5) when the TIT increased from 600 to 700 °C. The maximum heat addition $\Delta T$ increases when the TIT increases, however, the absolute changes in magnitude are different for each cycle. The heat addition $\Delta T$ of C6, C7 and C8 lie within the 1% integration penalty bounds listed in Table 2 and all the other cycle configurations studied fall outside of these bounds. It is safe to neglect C1 and C2 for detailed analysis as their heat addition $\Delta T$ and
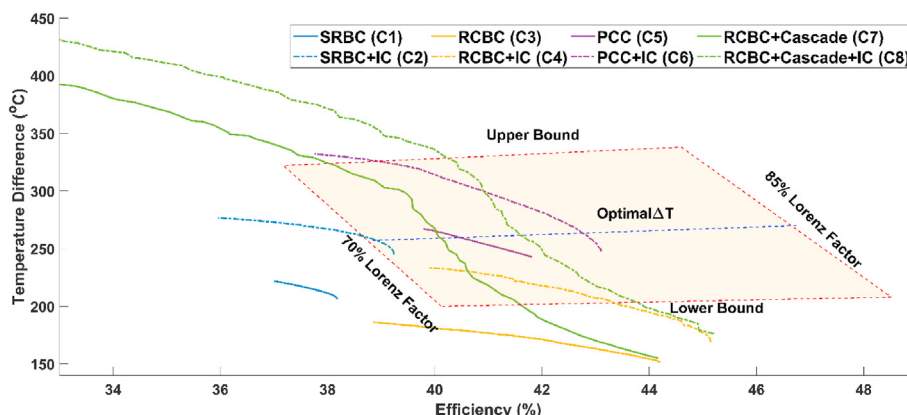


**Fig. 14.** Pareto fronts obtained from NSGA-II for CIT = 55 °C and TIT = 600 °C.
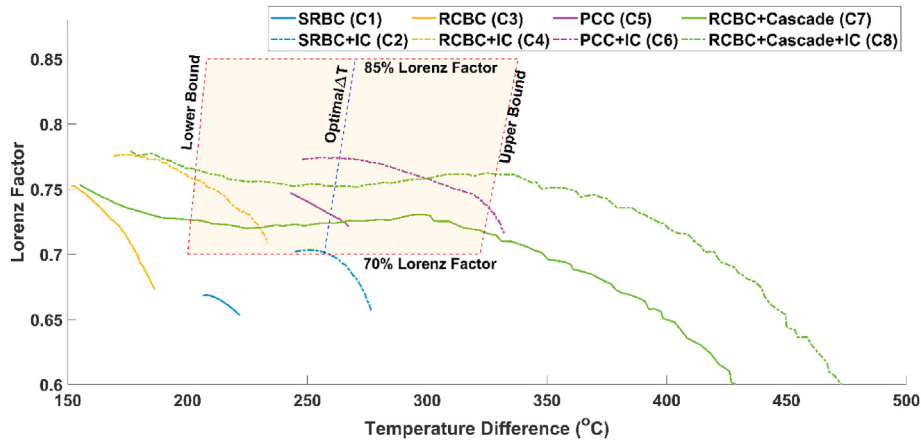
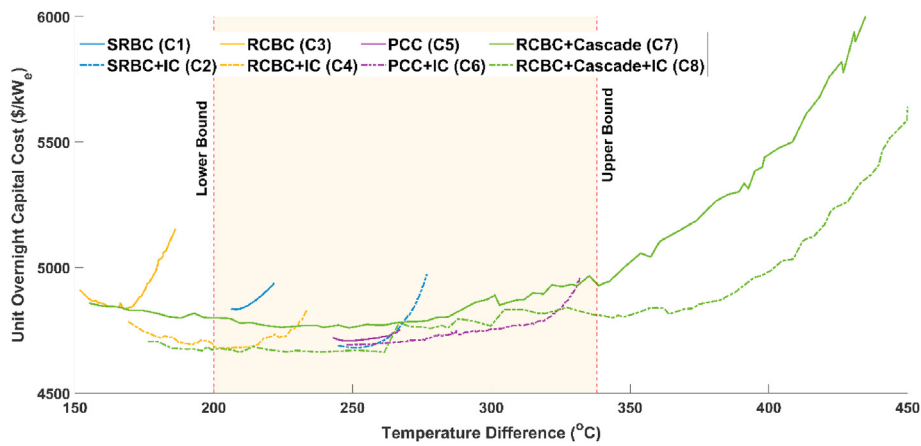**Fig. 15.** Lorenz factor across the Pareto front (shown in Fig. 14) for CIT = 55 °C and TIT = 600 °C.



**Fig. 16.** Overnight capital cost across the Pareto front (shown in Fig. 14) for CIT = 55 °C and TIT = 600 °C.
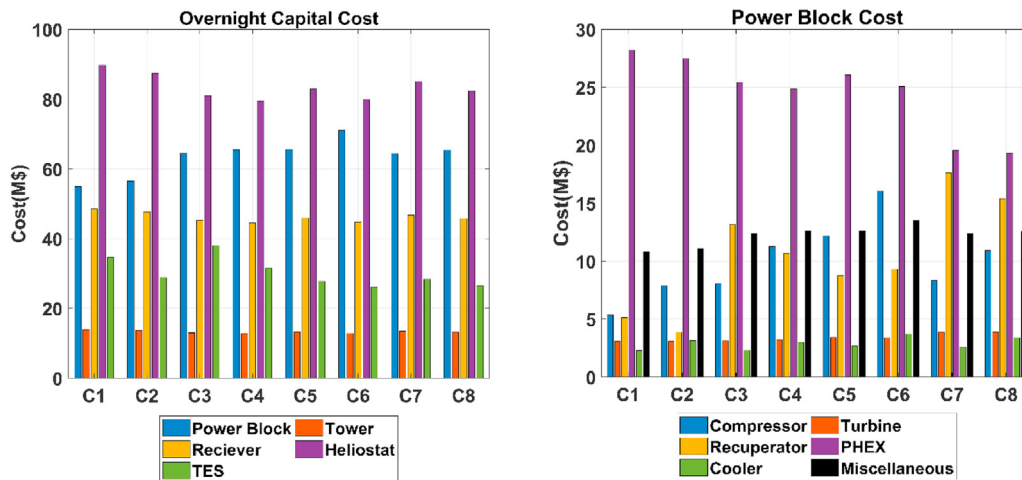


**Fig. 17.** Cost breakdown for CIT = 55 °C and TIT = 600 °C at the minimum overnight capital cost point: Left) Total capital cost Right) Power block cost breakdown.

efficiency are both lower and therefore highly unlikely to overcome the integration penalty solely with power block cost reduction. Similarly, C3 and C4 can be omitted as their heat addition ΔT is lower than 250 °C where the TES system cost increases monotonically (Fig. 5) therefore, this configuration cannot offset the integration penalty. Although heat addition ΔT of C5 falls outside the 1% integration penalty lower bound, the heat addition ΔT is higher than C7 and C8 at the maximum efficiency point. Furthermore, the power block cost of C5 is expected to be lower than C7 and C8 owing to the lower number of components, therefore, this
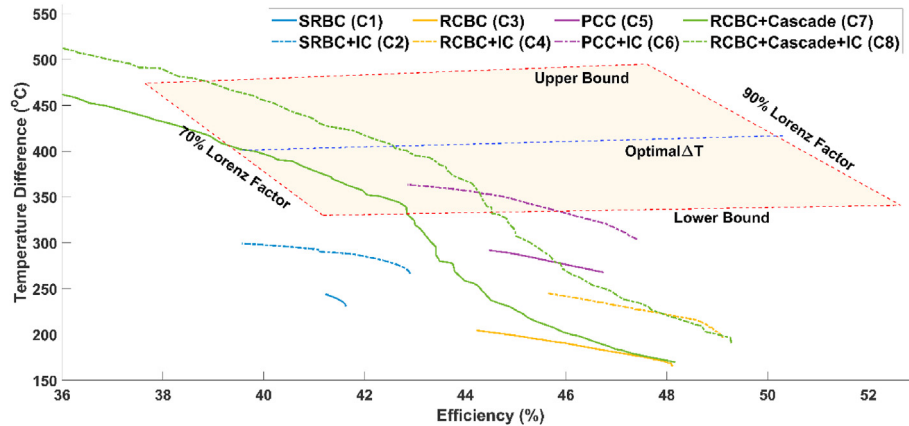
**Fig. 18.** Pareto fronts obtained from NSGA-II for CIT = 55 °C and TIT = 700 °C.

should still be considered for detailed analysis.

C6 achieved the highest Lorenz factor at the maximum efficiency point in comparison with all the other cycles owing to their reduced Lorenz efficiency because of higher heat addition ΔT (Fig. 19), however, the Lorenz factor of C8 increases when the heat addition ΔT is proximate to the optimal heat addition ΔT. The Lorenz factor of C7 and C8 are nearly plateaued over a larger range of heat addition ΔT then start to drop-off steeply. The optimal heat addition ΔT of an ideal cycle (Table 2) is about 410 °C, therefore, C6 and C8 may able to achieve higher cost reduction unless the power cycle cost of the other cycles offsets the cost penalty occurred from the solar field + TES integration.

The OCC across the Pareto front is shown in Fig. 20 and C8 achieved the lowest OCC followed by C6 as expected from the thermal performance. The minimum OCC of C6 is plateaued from its maximum efficiency point (minimum heat addition ΔT point in Fig. 20) and increases when the Lorenz factor starts to reduce steeply. The minimum OCC of all the cycles has increased within the range of 16.7% (C8) to 26.2% (C2) by increasing the TIT from 600 to 700 °C at 55 °C CIT. Likewise, the OCC increases from a minimum of 6.8% (C2) to a maximum of 15% (C7) due to the increase in CIT from 32 °C to 55 °C. The performance summary at the minimum OCC point are tabulated in the supplementary material (Section E.4).

Increasing the TIT from 600 to 700 °C also increases the cost of high temperature cycle components including PHEX and turbine (Fig. 21). The increase in the cost of the turbine is significant, for example, the turbine cost of C8 increases by 106.8% and C6

increases by 166.1%. The cost of PHEX of all the cycles increased compared to the equivalent 600 °C cases within a range of 1.1% (C5) to 10.3% (C7). Increasing the TIT also increased the OCC for all the cycles studied with a CIT of 55 °C, which may decrease in the future when the cost of the high-grade materials become cheaper or when the cost of high temperature TES system reduces which lowers the optimal integration heat addition ΔT.

### 3.3. Monte-Carlo uncertainty analysis

Since the cost function of the sCO$_2$ power block components are not N$^{th}$ of a Kind (NOAK), the uncertainty of them is still larger. Therefore, an uncertainty estimation is essential in order to foresee the range of OCC with the cumulative probability to reduce the financial risk. The cost functions uncertainty are listed in the supplementary material (Section E.5), and Monte-Carlo uncertainty analysis is performed at the minimum OCC points of all the cycles. The total number of samples considered in each cycle OCC estimation is 10,000.

From Fig. 22, it can be seen that the tCO$_2$ cycle (C9) has a lower cost for a CIT of 32 °C when the TIT is 600 °C whereas the cost of C9 is tentatively similar to the cost of C7 and C8 at the higher TIT of 700 °C. For a CIT of 55 °C, intercooled SRBC (C2) is preferred from the cycles studied when the TIT is 600 °C owing to its simple configuration, whereas C8 is attractive followed by C6 at the higher TIT of 700 °C. Intercooled cycles reduce the cost significantly for a CIT of 55 °C compared to cycles without intercooler whilst
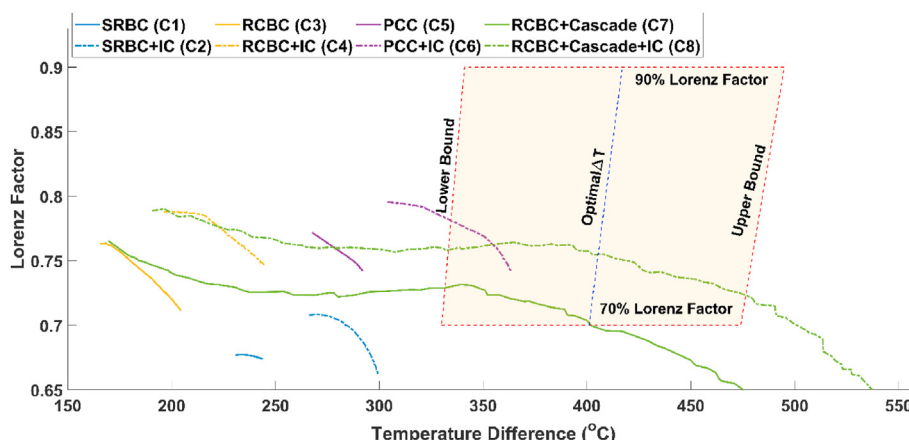


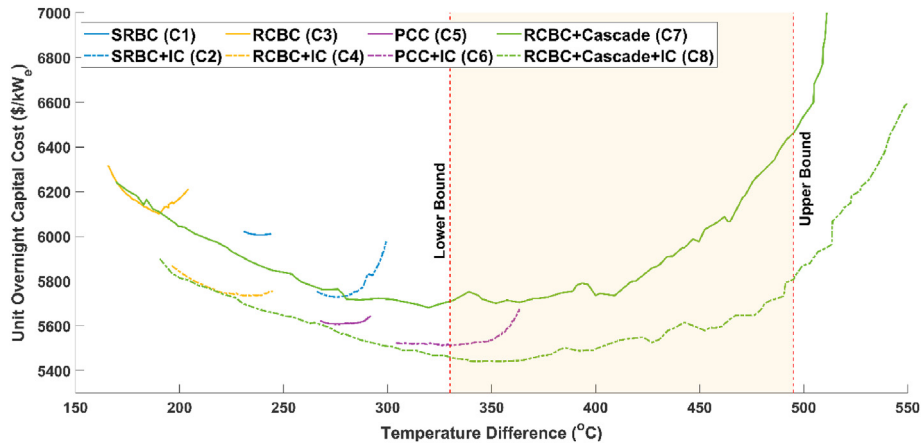**Fig. 19.** Lorenz factor across the Pareto front (shown in Fig. 18) for CIT = 55 °C and TIT = 700 °C.

**Fig. 20.** Overnight capital cost across the Pareto front (shown in Fig. 18) for CIT = 55 °C and TIT = 700 °C.
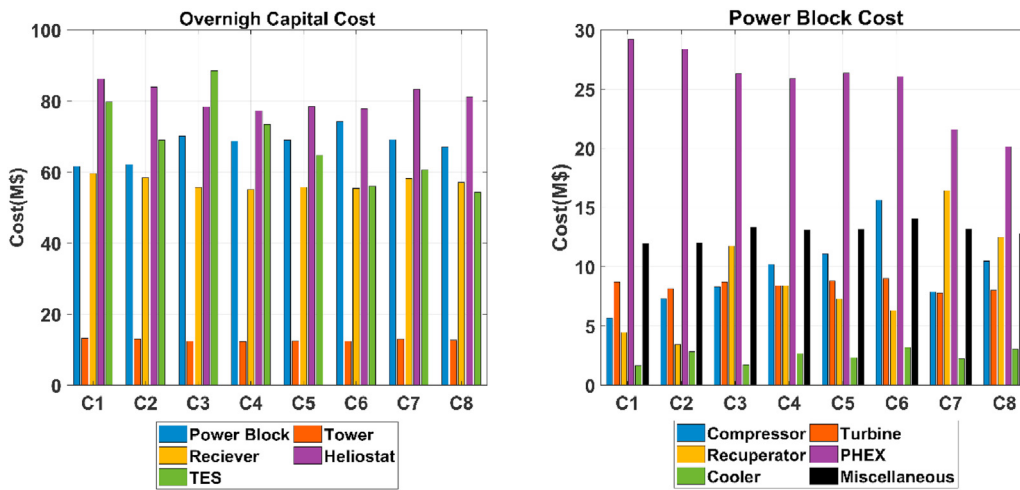


**Fig. 21.** Cost breakdown for CIT = 55 °C and TIT = 700 °C at the minimum overnight capital cost point: Left) Total capital cost Right) Power block cost breakdown.
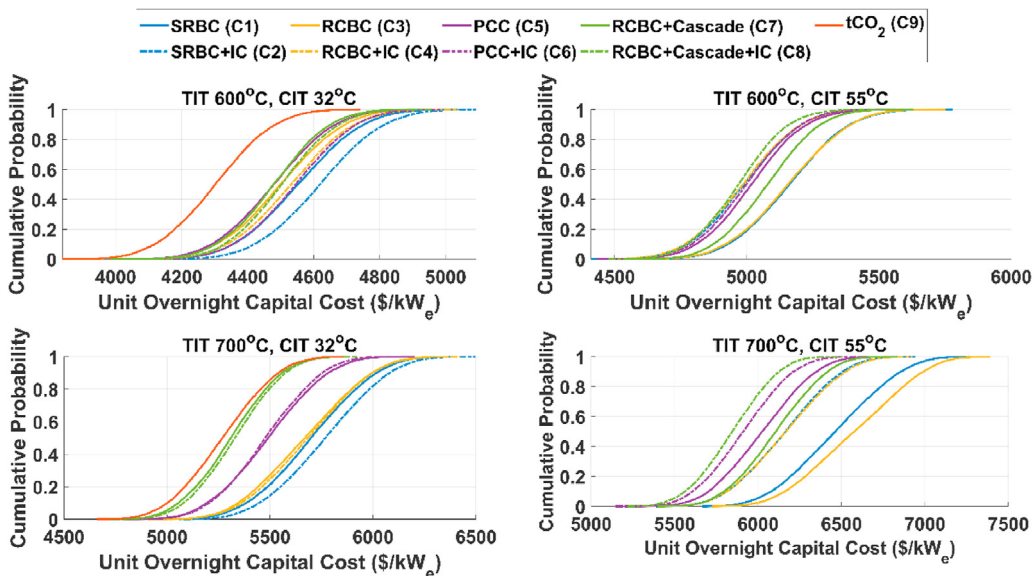


**Fig. 22.** Cumulative probability distribution of overnight capital cost per kW.

intercooler slightly increases the cost for a CIT of 32 °C.

## 4. Conclusions

Selection of an optimal sCO$_2$ cycle for a CSP application with a two-tank TES system was performed using multi-objective optimisation and nine sCO$_2$ cycles including two novel cycle configurations were investigated. The optimal molten salt temperature drop (heat addition ΔT) across the primary heat exchanger (PHEX) using an ideal power cycle was defined for different boundary conditions. The optimal heat addition ΔT of an ideal power cycle is about 270 °C for a TIT of 600 °C, which increases to about 420 °C for a TIT of 700 °C. This study identified that power cycle efficiency alone is not the primary driver from an economic perspective, especially if the maximum cycle efficiency is achieved away from the optimal heat addition ΔT. Screening the cycle configurations based on the power cycle efficiency without considering an optimal heat addition ΔT and Lorenz factor can lead to the selection of uneconomical cycle configurations. Cycle configurations that achieve a higher or lower heat addition ΔT compared to the optimal heat addition ΔT need to overcome an integration penalty caused by the CSP and TES systems to become economically attractive.

Addition of an intercooler is recommended for a CIT of 55 °C whereas this may not be economically justified for a CIT of 32 °C. Increasing the TIT from 600 to 700 °C also increased both the power block and overnight capital cost (OCC). In order to realise a cost reduction for a TIT≥700 °C either 1) the storage system cost must be reduced, which reduces the optimal heat addition ΔT, or 2) novel cycle configurations must be developed that achieve higher efficiency proximate to the optimal heat addition ΔT without increasing the power block cost. For a higher TIT, splitting the PHEX into two (or more) in series, where difference grade of materials can be adopted, is recommended to reduce the cost.

Among the cycle configurations investigated, the simple recuperative cycle with intercooler (C6) is attractive when the CIT is 55 °C for a TIT of 600 °C whereas the novel recompression cycle + cascade cycle with intercooler (C8) is attractive for a TIT of 700 °C (i.e. 10.8% reduction in cost compared to recompression cycle). The partial cooling cycles show promising economic performance for a TIT of 700 °C compared to recompression cycle. The transcritical CO$_2$ (tCO$_2$) cycle shows high potential primarily due to its lower power block cost.

## Credit author statement

Dhinesh Thanganadar—Conceptualization, Formal analysis, Investigation, Methodology, Software, Writing − original draft, Francesco Fornarelli– Data curation, Methodology, Software, Validation, Writing − review & editing, Sergio Camporeale– Data curation, Methodology, Supervision, Visualization, Writing − review & editing, Faisal Asfand– Conceptualization, Formal analysis, Investigation, Writing − review & editing, Jonathon Gillard − Formal analysis, Investigation, Writing − review & editing, Kumar Patchigolla—Conceptualization, Funding acquisition, Supervision, Writing − review & editing.

## Declaration of competing interest

The authors declare that they have no known competing financial interests or personal relationships that could have appeared to influence the work reported in this paper.

## Acknowledgement

The author would like to thank Mr. David Dewis, Principle

## Appendix A. Supplementary data

Supplementary data to this article can be found online at https://doi.org/10.1016/j.energy.2021.121755.

## References

[1] IRENA. Renewable. Energy technologies: cost analysis series - concentrating solar power, vol. 1; 2012. https://doi.org/10.1016/B978-0-12-812959-3.00012-5.

[2] Mehos M, Turchi C, Vidal J, Wagner M, Ma Z, Ho C, et al. Concentrating solar power Gen3 demonstration roadmap. 2017.

[3] Mehos M, Turchi C, Jorgenson J. Advancing concentrating solar power technology, performance, and dispatchability. SunShot 2016:1−66. https://doi.org/10.1016/B978-0-08-087872-0.00319-X.

[4] Dostal V, Driscoll MJ, Hejzlar P. A supercritical carbon dioxide cycle for next generation nuclear reactors. MIT-ANP-TR-100; 2004.

[5] Le Moullec Y. Conceptual study of a high efficiency coal-fired power plant with CO$_2$ capture using a supercritical CO$_2$ Brayton cycle. Energy 2013;49: 32−46. https://doi.org/10.1016/j.energy.2012.10.022.

[6] Thanganadar D, Asfand F, Patchigolla K, Turner P. Techno-economic analysis of supercritical carbon dioxide cycle integrated with coal-fired power plant. Energy Convers Manag 2021;242:114294. https://doi.org/10.1016/j.enconman.2021.114294.

[7] Thanganadar D, Asfand F, Patchigolla K. Thermal performance and economic analysis of supercritical Carbon Dioxide cycles in combined cycle power plant. Appl Energy 2019;255:113836. https://doi.org/10.1016/j.apenergy.2019.113836.

[8] Poerner M, Rimpel A. Waste heat recovery. Elsevier Ltd; 2017. https://doi.org/10.1016/B978-0-08-100804-1.00010-4.

[9] Li H, Yang Y, Cheng Z, Sang Y, Dai Y. Study on off-design performance of transcritical CO$_2$ power cycle for the utilization of geothermal energy. Geothermics 2018;71:369−79. https://doi.org/10.1016/j.geothermics.2017.09.002.

[10] Crespi F, Gavagnin G, Sánchez D, Martínez GS. Supercritical carbon dioxide cycles for power generation: a review. Appl Energy 2017;195:152−83. https://doi.org/10.1016/j.apenergy.2017.02.048.

[11] Turchi CS, Ma Z, Neises T, Michael W. Thermodynamic study of advanced supercritical carbon dioxide power cycles for high performance concentrating solar power systems. In: Proc. ASME 2012 6th int. Conf. Energy sustain.; 2012. p. 375−83. https://doi.org/10.1115/ES2012-91179.

[12] Crespi F, David S, Mart GS. Analysis of the thermodynamic potential of supercritical carbon dioxide cycles : a systematic approach. ASME Turbo Expo 2017:1−14. https://doi.org/10.1115/GT2017-64418.

[13] Angelino G. Real gas effects in carbon dioxide cycles. ASME- Pap 69-Gt-102 1969:1−12. doi:10.1115/69-GT-102.

[14] Thanganadar D, Fornarelli F, Camporeale S, School Gillard J, Patchigolla K. Design performance analysis of supercritical CO$_2$ cycle for CSP application with sensible heat thermal storage. Proc. ASME Turbo Expo 2021 Turbomach. Tech. Conf. Expo. 2021:1−10.

[15] Crespi F, Sánchez D, Sánchez T, Martínez GS. Capital cost assessment of concentrated solar power plants based on supercritical carbon dioxide power cycles. J Eng Gas Turbines Power 2019;141:1−9. https://doi.org/10.1115/1.4042304.

[16] Crespi F, Sánchez D, Rodríguez JM, Gavagnin G. A thermo-economic methodology to select sCO$_2$ power cycles for CSP applications. Renew Energy 2020;147:2905−12. https://doi.org/10.1016/j.renene.2018.08.023.

[17] Thanganadar D, Fornarelli F, Camporeale S, Asfand F, Patchigolla K. Analysis of design, off-design and annual performance of supercritical CO$_2$ cycles for CSP application. Proc. ASME Turbo Expo 2020:2020.

[18] Thanganadar D, Fornarelli F, Camporeale S, Asfand F, Patchigolla K. Off-design and annual performance analysis of supercritical carbon dioxide cycle with thermal storage for CSP application. Appl Energy 2021;282:116200. https://doi.org/10.1016/j.apenergy.2020.116200.

[19] Wright S, Tom C, Edward P, Tom L, Gary R, J S-Aa. Summary of the sandia supercritical CO$_2$ development program. Boulder, Colorado: Int. SCO2 Power Cycle Symp.; 2011.

[20] Lecompte S, Ntavou E, Tchanche B, Kosmadakis G, Pillai A, Manolakos D, et al.

Review of experimental research on supercritical and transcritical thermodynamic cycles designed for heat recovery application. Appl Sci 2019;9:1−26. https://doi.org/10.3390/app9122571.

[21] Black & Veatch. Molten salt concept definition & capital cost estimate. Prepared for SunShot U.S. Department of Energy; 2016. https://doi.org/10.2172/1335150.

[22] Kolb GJ, Ho CK, Mancini TR, Gary JA. Power tower technology roadmap and cost reduction plan. Conc Sol Power Data Dir an Emerg Sol Technol 2012: 223−50.

[23] Kelly B, Kearney D. Thermal storage commercial plant design study for a 2-tank indirect molten salt system final report. National Renewable Energy Laboratory (NREL); 2006. p. 1−32.

[24] Ho CK, Carlson M, Garg P, Kumar P. Cost and performance tradeoffs of alternative solar-driven S-CO2 brayton cycle configurations. Proc. ASME 2015 Power Energy Convers. Conf. 2015:1−10. https://doi.org/10.1016/j.jhydrol.2013.03.030.

[25] Dunham MT, Iverson BD. High-efficiency thermodynamic power cycles for concentrated solar power systems. Renew Sustain Energy Rev 2014;30: 758−70. https://doi.org/10.1016/j.rser.2013.11.010.

[26] Johnson GA, McDowell MW, O'Connor GM, Sonwane CG, Subbaraman G. Supercritical CO2 cycle development at pratt & whitney rocketdyne. Proc ASME Turbo Expo 2012;5:1015−24. https://doi.org/10.1115/GT2012-70105.

[27] Kimzey G. Development of a Brayton bottoming cycle using supercritical carbon dioxide as the working fluid. 2012.

[28] Angelino G. Carbon dioxide condensation cycles for power production. J Eng Gas Turbines Power 1968;90:287−95. https://doi.org/10.1115/1.3609190.

[29] H. Supercritical CARbon dioxide/alternative fluids blends for efficiency upgrade of solar power plants. 2019. https://cordis.europa.eu/project/id/814985. [Accessed 15 May 2020].

[30] Crespi F, Sánchez D, Rodríguez JM, Gavagnin G. Fundamental thermo-economic approach to selecting sCO2 power cycles for CSP applications. 4th Int. Semin. ORC Power Syst. 2017;129:963−70. https://doi.org/10.1016/j.egypro.2017.09.215.

[31] Lewis J, Clementoni EM, Cox TL. Effect of compressor inlet temperature on cycle performance for a supercritical carbon dioxide brayton cycle. 6th Int. Supercrit. CO2 Power Cycles Symp. 2018;9:2−10. Pittsburgh, Pennsylvania.

[32] Clementoni EM, Cox TL. Effect of compressor inlet pressure on cycle performance for a supercritical carbon dioxide brayton cycle. Proc. ASME Turbo Expo 2018;9:1−8. https://doi.org/10.1115/GT2018-75182. Oslo, Norway.

[33] Asfand F, Thanganadar D, Patchigolla K. Thermodynamic performance of a supercritical CO2 cycle integrated with a recuperative absorption cooling system. ECOS 2019 - Proc. 32nd Int. Conf. Effic. Cost, Optim. Simul. Environ. Impact Energy Syst. 2019;2019− June:3895−903. WROCLAW, POLAND.

[34] Hacks AJ, Schuster S, Brillert D. Stabilizing effects of supercritical CO2 fluid properties on compressor operation. Int J Turbomachinery, Propuls Power 2019;4. https://doi.org/10.3390/ijtpp4030020.

[35] Lemmon EW, Huber ML, McLinden MO. NIST standard reference database 23. Natl Inst Stand Technol 2013;9.1.

[36] Black JB. Cost and performance baseline for Fossil energy plants volume 3b: low rank coal to electricity: combustion cases, vol. 3; 2011.

[37] Deb K, Pratap A, Agarwal S, Meyarivan T. A fast and elitist multiobjective genetic algorithm: NSGA-II. IEEE Trans Evol Comput 2002;6:182−97. https://doi.org/10.1109/4235.996017.

[38] Weiland NT, Lance BW, Pidaparti SR. SCO2 power cycle component cost correlations from DOE data spanning multiple scales and applications. Proc. ASME Turbo Expo 2019;9:1−17. https://doi.org/10.1115/GT2019-90493.

[39] Couper JR, Penney WR, Fair JR, Walas SM. Chemical process equipment: selection and design. Third Edit; 2012. https://doi.org/10.1016/B978-0-12-396959-0.00025-2.

[40] Carlson MD, Middleton BM, Ho CK. Techno-economic comparison of solar-driven sCO2 brayton cycles using component cost models baselined with vendor data. Proc ASME 2017 Power Energy Conf 2017:1−7. https://doi.org/10.1115/ES2017-3590.

[41] Mehos M, Turchi C, Vidal J, Wagner M, Ma Z, Ho C, et al. Concentrating solar power Gen3 demonstration roadmap. Nrel/Tp-5500-67464 2017:1−140.

[42] Ma Y, Morosuk T, Luo J, Liu M, Liu J. Superstructure design and optimization on supercritical carbon dioxide cycle for application in concentrated solar power plant. Energy Convers Manag 2020;206:112290. https://doi.org/10.1016/j.enconman.2019.112290.

[43] Ho CK, Iverson BD. Review of high-temperature central receiver designs for concentrating solar power. Renew Sustain Energy Rev 2014;29:835−46. https://doi.org/10.1016/j.rser.2013.08.099.

[44] Ennio Macchi MA. Organic rankine cycle (ORC) power systems: technologies and applications. first ed. Woodhead Publishing; 2016.

[45] Can Gülen S, Joseph J. Combined cycle off-design performance estimation: a second-law perspective. J Eng Gas Turbines Power 2012;134:1−11. https://doi.org/10.1115/1.4004179.